JOURNAL OF AIRCRAFT
Vol. 36, No. 1, January–February 1999

Optimization of Waverider-Based Hypersonic Cruise Vehicles with Off-Design Considerations

Naruhisa Takashima* and Mark J. Lewis†
University of Maryland, College Park, Maryland 20742-3015

A waverider-based hypersonic vehicle is optimized for a Mach 10 cruise mission. Issues related to optimization of a fully integrated hypersonic engine–airframe combination are reviewed. In contrast to previous optimizations presented for waverider-based designs, the current approach takes into account certain aspects of the off-design performance. The design is optimized for maximum range along a 1000-psf dynamic pressure trajectory from Mach 6 to Mach 10 under scramjet propulsion. A so-called osculating cone waverider forebody is chosen so that it generates uniform flow for the two-dimensional multiple-ramp inlet design. The flow through the scramjet engine is modeled analytically, including effects of mixing and combustion. The vehicle model is validated with computational fluid dynamics calculations. Both the inlet and the nozzle shapes as well as the overall airframe configuration are optimized for maximum range along the trajectory using the method of sequential quadratic programming. The difference in the range performance of the present design and a design that has been optimized at a fixed Mach 10 cruise condition is less than 1%. This suggests that previous single-point designs will in fact perform well across the hypersonic portion of the flight envelope.

Nomenclature

a = acceleration
C_D = drag coefficient
C_L = lift coefficient
C_M = pitching-moment coefficient
C_T = thrust coefficient
c_p = specific heat at constant pressure
c_v = specific heat at constant volume
h = altitude
I_{sp} = specific impulse
L/D = lift-to-drag ratio
L/W = lift-to-weight ratio
M = Mach number
m = mass of vehicle
$\dot{m}_f$ = fuel mass flow rate
P = pressure
q_∞ = freestream dynamic pressure
R = gas constant, also range
R_{cruise} = cruise range
S_{ref} = reference area
T = temperature
T/D = thrust-to-drag ratio
T_{net} = net thrust
V_∞ = velocity
W = weight of the vehicle
x_l = mixing length
α = angle of attack
β = waverider conical shock angle
γ = specific heat ratio
δ = control-surface deflection angle
η_{mix} = mixing efficiency
θ_h = heat release parameter
ρ = density
ϕ = fuel equivalence ratio
ϕ_r = reacting fuel equivalence ratio

Received April 15, 1998; revision received Aug. 9, 1998; accepted for publication Aug. 9, 1998.

*Graduate Research Assistant; currently Aerospace Engineer, Astrox Corporation, 1350 Piccard Drive, Suite 320, Rockville, MD 20850. Member AIAA.

†Associate Professor, Department of Aerospace Engineering. Associate Fellow AIAA.

Introduction

AIR-BREATHING hypersonic vehicles, powered by supersonic combustion ramjets, or scramjets, have been considered for flight in the missile and cruiser range of Mach 6–12, or with application to accelerators operating up to orbital speeds beyond Mach 25. The successful design of such craft will depend on the implementation of weight-saving, low-drag, engine-integrated airframes, in which the external vehicle surfaces act as components of the propulsion system. In a concept that has been incorporated into several hypersonic design studies, including those associated with the now-canceled National Aerospace Plane program and the NASA-sponsored McDonnell Douglas Dual Fuel Mach 10 cruiser study, the aircraft forebody would serve as the engine compression surface, and the aftbody would act as the engine nozzle.[1–3] In a sense, the entire vehicle undersurface comprises the propulsion system, and it is difficult to consider the propulsive pressure field as being separate from the overall lift and drag forces.

One of the implications of this engine–airframe integration is that the forebody must be properly shaped to provide compression that satisfies the requirements of the hypersonic engine, and the aftbody must function as an efficient nozzle. Conversely, because engine forces will be distributed along the vehicle undersurface, the airframe lift and drag, and trim and control requirements, will depend directly on the engine characteristics. There is thus a strong coupling between the external vehicle aerodynamics and the performance of a hypersonic engine system. There is also likely to be greater use of engine exhaust flow for lift, particularly in cruiser applications, as compared with designs at lower speed regimes. Because of the complexity of these interactions and the narrow thrust margins available with an air-breathing hypersonic engine, the entire engine–airframe system should be properly optimized for maximum overall mission performance as a fully integrated system.

Engine thrust depends on the ingested mass flow (and, thus, capture area and flight dynamic pressure), engine placement, and forebody dimensions. Because the vehicle forebody is acting as the engine inlet, the flow properties entering the engine

proper must be acceptable for combustion, which means that they must satisfy very narrow requirements for pressure and temperature if combustion is to be realized at a sufficiently high rate in the supersonic flow. Additionally, it is desirable for the forebody to be nearly two dimensional, so that the boundary layer will remain laminar for as long as possible before entering the engine, to reduce skin friction.[4] Whether or not the forebody boundary layer can be diverted, it is generally considered desirable to have minimal gradients in mass flux, pressure, and temperature inside the combustor, again dictated by the inlet flowfield.

As the name implies, scramjets operate in a manner similar to that of traditional ramjet engines, though with supersonic flow through all or most of the combustor. Flow enters an inlet, fuel is mixed and burned in a combustor, and the resulting heated flow accelerates through a nozzle to provide useful thrust, with performance that was first characterized by Weber and MacKay.[5] In the ramjet, the inlet decelerates the flow to subsonic speeds for the combustor, thereby increasing residence time for efficient mixing and burning and reducing combustor total pressure losses. In contrast, in the scramjet, the inlet flow is not decelerated to low subsonic speed as it enters the combustion process; inlet shocks are primarily used to raise the static temperature and pressure to ignition conditions. Traditional ramjets have poor thrust performance beyond Mach 6, as the combustor inlet temperature, which is nearly equal to inlet stagnation temperature, approaches the limiting equilibrium combustion temperature. With supersonic flow throughout, the static temperature of the scramjet is always below the stagnation temperature, which allows for the release of combustion energy at Mach numbers in excess of 6 or above. In delivering supersonic flow to the combustor, inlet shock waves are weaker than they would be with subsonic flow, though losses caused by heating in the combustor are increased.

The design of a practical scramjet is complicated by the rapid flow through the engines and the comparative difficulty of mixing in a supersonic stream, the result of which is residence times that are comparable with mixing and combustion time scales. Even if the fuel can be sufficiently mixed into the stream, the rate of the subsequent combustion process will be very sensitive to the ambient temperature and pressure of the flow stream. From the early work of Ferri[6] to the more recent work of Rogers and Schexnayder,[7] it has been found that the hydrogen–oxygen reaction rate scales in approximate proportion to the 1.7 power of pressure, and exponentially with temperature. Delivering positive thrust with a reasonable reaction length in a scramjet engine requires static conditions of at least $\frac{1}{4}$ atm and 1000 K, as Paull et al.[8] have demonstrated in an extensive series of shock-tunnel experiments. However, inlet temperatures above about 1500 K will result in unacceptable reductions in available combustion energy release, because the final combustion temperature is limited by the hydrogen–oxygen equilibrium dissociation temperature of about 3200 K. These limits can be modified by the addition of additives such as silane or peroxide, but this will entail more complicated, and more dangerous, engine designs. The same arguments apply to hydrocarbon fuels, even though energy release rates and equilibrium temperatures are lower than those of hydrogen.

These considerations will have a fundamental impact on the required length of a scramjet combustor, and thus, its length relative to the rest of the vehicle. At 1000 K and 1 atm, characteristic times for an efficient unenhanced hydrogen–oxygen combustion reaction will be less than 1 ms. Thus, at a typical hypersonic velocity of Mach 10, the combustor would be approximately 3 m long,[9] although even shorter reaction lengths, both with and without combustion and mixing enhancement, have been reported.[8] Any reduction in the reaction rate will result in the requirement for a longer, heavier combustor with more internal losses, or incomplete combustion will result. Associated with all of these preceding questions is the fundamental issue of where to properly place a propulsion system on the hypersonic configuration, to provide untrimmed balance, good inlet mass capture, and nozzle lift.

Various efforts have examined the multidisciplinary coupling issues associated with scramjet-powered vehicles. For instance, O'Neill and Lewis[10] presented a complete methodology that includes propulsion, airframe, structure, and mission analysis for a wide range of hypersonic vehicle concepts. Others have examined specific coupling issues in detail; e.g., Raney et al.[11] studied the aeroelastic and propulsive interactions on a hypersonic craft operating at Mach 6 and 10, considering structural bending modes.

Several studies have examined the application of optimization techniques to hypersonic vehicle configurations. One rigorous approach to the optimization of this class of vehicles has been demonstrated by McQuade et al.,[12] who used a full computational solution, rather than analytical or semianalytical techniques, to optimize the propulsive flow path of relatively simple, though appropriately representative, scramjet-powered configurations for maximum net thrust. This approach is two dimensional, but actual scramjet flow paths are indeed likely to be as two dimensional as possible, particularly on inlet and nozzle, to control inlet flow thermodynamics, minimize crossflow, and delay boundary-layer transition on the forebody.[4] Recent improvements in computational efficiency have been directed specifically at the application to complex hypersonic configurations, offering the promise that future optimization codes may be able to use even more realistic computational solutions. For instance, Payne and Walker[13] coupled a full Navier–Stokes code with a parabolized Navier–Stokes code for realistic complex hypersonic configurations.

A similar effort in optimization with computational fluid dynamics by Sabean and Lewis[14] was applied to the identification of axisymmetric shapes with maximum thrust for a scramjet-powered projectile. In that effort, methane combustion was included in a computational optimization process that used the methodology of Baysal and Eleshaky[15] in the hypersonic realm, but run-time considerations prevented the inclusion of viscous effects. Baysal and Eleshaky optimized three-dimensional aerodynamic forms, including hypersonic shapes, using a technique that directly calculates sensitivites of the first-order-accurate discretized Euler equations. This work was applied to major components, i.e., a scramjet nozzle aftbody, and incorporates the method of Vanderplaats.[16] Though an important contribution in reducing the computational costs of optimization, the run times required for a full three-dimensional, engine-integrated geometry are still daunting.

This present work focuses on optimization with a different approach to the coupled vehicle–airframe problem, an inverse one in which the calculation requirements are reduced by the use of known flowfields. Foster and Dulikravich[17] and Dulikravich and Sheffer[18] demonstrated inverse approaches to hypersonic aerodynamic shapes, including minimum-drag bodies. A similar inverse approach was used by Sabean et al.[19] to produce star-shaped bodies based on so-called waverider segments to optimize for minimum drag, though without propulsion. O'Neill and Lewis[9] first demonstrated that an entire three-dimensional engine–airframe integrated scramjet-powered vehicle can be derived with an inverse analytical approach from waverider shapes. Kothari et al.[20] showed that a similar approach can be taken with the inward-turning class of inlets.

The present work builds on the initial results of O'Neill and Lewis,[9] in which cruiser vehicles were optimized to provide maximum range under various fixed flight conditions, with specified inlet conditions, and constrained so that lift equals weight. Accelerators were optimized for maximum net thrust; for a cruiser, net thrust is zero at cruise conditions, and it is most desirable to maximize range, which is proportional to the specific impulse time lift-to-drag ratio. The results of this effort show that engine performance, as well as the choice of the mission-oriented objective function, can have a strong impact on the optimized vehicle design. For instance, optimizing the

configuration for an accelerator objective results in a vehicle with shorter nozzles and larger engine spans, as compared with cruise configuration, which trade some of their engine propulsive force for lift. Thus, it is not correct to simply maximize L/D while independently maximizing I_{sp} for a cruiser; rather, it is important to optimize their combined effect on range.

Cruise vehicle studies detailed in O'Neill and Lewis,[9] Tarpley and Lewis,[21] and the work reported here, have depended on the use of waveriders because of the ease of computing and specifying their associated flowfields, as well as their good aerodynamic efficiency. Waveriders are supersonic shapes in which the bow shock wave is directly attached to the leading edge. This means that all of the flow that passes through the shock wave on the lower lifting part of the waverider is contained below the waverider. This has the benefit of producing a generally high value of available L/D with high lift, and reducing crossflow and nonuniformities on the compression surface.

Nonweiler[22] first demonstrated that waveriders can be defined from known flowfields. He used a simple two-dimensional wedge to generate a flow with a known shock wave, then picked a surface parallel to the direction of flow under the wedge to represent the lower surface of his waverider. The intersection of that lower surface and the original shock wave defines the leading edge with an attached shock wave. This whole process works because the flowfield is mathematically hyperbolic, so that the carved-out section that forms the waverider surface, representing perhaps a small portion of the original flowfield, still retains the properties of that flowfield, even though the generating body has been ignored once the waverider is defined.

Other generating bodies can also be used as the starting point of the waverider flowfield design process. Rasmussen and Clement[23] worked extensively with conically derived waveriders, which tend toward higher volumetric efficiency than the wedge-derived forms. For a given flight Mach number, both the wedge and cone-shaped forms have only one degree of freedom: the oblique surface angle. The original work of O'Neill and Lewis[9] and Emanuel and Park[24] used conically derived forms for the forebody compression surfaces of engine-integrated vehicles. Gillum and Lewis[25] tested conically derived shapes that were optimized with volumetric considerations, to produce vehicle forms that strike an acceptable compromise between aerodynamics and packaging, and with realistic, rounded leading edges. In fact, nearly any shape that has a shock wave and supersonic downstream flow associated with it can be used as the initial generating body for a waverider. In turn, each generating flowfield contains an infinite number of stream surfaces that can be selected to form the final waverider, so there is great flexibility in the process, and it is ready for the application of optimization.

Numerous studies, including both experimental and computational, have shown that waverider shapes, though derived at a single flight condition, have acceptable performance at off-design.[25,26] It has also been shown that other considerations, besides simple aerodynamics and volume, can be included in an optimization of the objective function using the same inverse approach. For instance, Tarpley and Lewis[21] showed the effects of steady-state flight and static margin constraints on the optimized design on an engine-integrated wedge-derived waverider. The performance of the optimized vehicle, which included the steady-state flight constraints, is significantly greater than the performance of the vehicle optimized with no steady-state flight constraints, assuming that control-surface deflections must be included for trim.

Ideally, the design of a hypersonic vehicle, which includes the engine design, should be optimized for the entire trajectory, from takeoff to landing. Even for a cruise-type application, when considerable time is spent at a fixed flight condition, the performance requirements at nonhypersonic speeds, such as at transonic speeds when the thrust pinch occurs, or even at off-design hypersonic speeds when the engine transitions from a ramjet mode to a scramjet mode, may have a significant impact on the overall design. At low speeds, the large inlet and nozzle areas required for hypersonic flight can cause a significant amount of drag. Furthermore, for a mixed-mission cruise scenario, which may involve flight at several different sustained Mach numbers, it is not even obvious which is the best design point to select. Although the software and hardware are available to accomplish this task, from a practical standpoint it remains difficult to implement. Nonetheless, it has been shown by previous works that valuable information can be still be gained by performing optimization, even at a fixed condition.

In this study, the design of a Mach 10 cruiser with an inlet forebody that is based on a so-called osculating cone waverider, with a flowfield constructed from numerous slices of conical flow, is optimized along a hypersonic trajectory for maximum range. The method of generating an osculating cone waverider is described next. Off-design supersonic aerodynamic forces are calculated analytically and included in the optimization process. The scramjet engine performance is determined by a quasi-one-dimensional combustor model with partial equilibrium combustion, and the two-dimensional nozzle flow is calculated using a method of characteristics.

Method of Osculating Cones

Given that hypersonic waveriders are generally designed using an inverse process in which a flowfield is first selected around a chosen generating body, an intriguing question is: what is the best generating shape to use in forming that initial generating flowfield? Because the waverider is generated from only a portion of the flowfield, the characteristics of the generated waverider shape may not necessarily reflect the characteristics of the generating shape. For a waverider shape that is part of an integrated air-breathing hypersonic vehicle, this becomes an even more difficult question. The wedge-derived forms can provide highly uniform flow to the inlet ramps; however, the aerodynamic performance as well as the volumetric efficiencies tend to be poor. In contrast, waverider shapes generated from axisymmetric flowfields have better aerodynamic performance with greater volumetric efficiency; however, the flow coming off the forebody is no longer uniform, and for a given inlet width, the mass capture area is smaller. Furthermore, an axisymmetric forebody/inlet combination requires greater turning angles and contraction ratio for a given pressure rise, which can increase the cross-sectional area of the vehicle.

Hence, what is truly desired is a generating flowfield that can generate a waverider shape with the positive attributes of the waveriders derived from the two generating flowfields. One option is to use a hybrid geometry for the generating shape. For instance, a hybrid cone–wedge shape was used to successfully generate a waverider that has a uniform forebody flow, such as a wedge-derived waverider, but with a good volumetric efficiency, like a conically derived shape.[27] The hybrid shape introduces extra flexibility into the waverider optimization process by allowing the optimizer to expand or contract the dimension of the wedge segment relative to the cone, and therefore, make the flowfield more wedge-like or cone-like. However, because this method requires a three-dimensional Euler calculation for each generating body, it is not particularly well suited for preliminary vehicle design study, which may require the exploration of numerous different shapes. Most recently, work has concentrated on an even more promising technique that eliminates the need to choose a generating body and permits direct specification of the desired shock wave instead. This is the so-called osculating (Latin for kissing) cones waverider method, developed originally by Sobieczky et al.[28]

In the method of osculating cones, the generating flow is defined by a design Mach number, a bow shock angle, and a shock-wave shape at the exit plane of the waverider; hence,

the method does not require a generating body to be defined. The flowfield behind the nonaxisymmetric shock is determined by assuming locally conical flow in the normal planes along the shock curve. The locally conical flow is defined by an osculating plane, as shown in Fig. 1. The shock angle as well as the Mach number that define the locally conical flow are kept constant in each osculating plane to ensure a smooth continuous lower surface on the generated waverider shape. The vertex of the conical flowfield in each plane is determined by the local radius of curvature and the shock angle. The shock curve is chosen so that the change in the radius of curvature is continuous along the curve, and a series of planes is used along the shock curve in the exit plane to fully define the flowfield behind the bow shock.

Note that in the limit of infinite radius of curvature, the conical flow degenerates into a wedge flow, so that by prescribing a flat shock curve, a wedge caret-wing waverider can be generated with the osculating cone method. Similarly, a conical waverider can be generated by simply prescribing a shock curve with constant radius of curvature, i.e, a circular arc. Thus, by choosing a shock curve that has an infinite radius of curvature along the center region and a finite radius of curvature along the outboard region, the positive attributes of the two generating flowfields, a wedge flow and a conical flow, can be combined in a single waverider.

Because the flowfield is assumed to be locally axisymmetric, the method can be inaccurate when large spanwise pressure gradients are present; however, such a flow would have a corresponding shape with large surface curvature, which would likely not be suitable for practical applications. Moreover, the integrated aerodynamic forces calculated by the method matched well with the values calculated numerically.[27] More importantly, the flexibility provided by the technique has already been shown to produce shapes with superior aerodynamic and volumetric performance compared with the simpler wedge- and cone-derived forms, and the greater flexibility also enables the waverider forebody shape to match an engine flow path or general shape of an existing, generic geometry.[27,29] This is most useful for comparing waverider shapes to an existing, nonoptimized configuration, or to match a waverider aerodynamic shell to an existing vehicle.

Once the generating flowfield is established, an osculating cone waverider shape is determined by selecting a leading edge at the exit plane. When choosing a leading-edge curve, the leading-edge curve must intersect all of the osculating plane to have the prescribed shock curve in the exit plane, and the distance between a leading-edge point and the corresponding point along the shock curve must decrease from the centerline to the wing tip to avoid a forward-swept wing. When the vertex of the osculating cone and the leading-edge point is determined, the lower surface of the waverider can be constructed by tracing the streamline along a known conical flow, analogous to the generation of a conical waverider. If the shock curve is flat, i.e., the radius of curvature is infinite, the slope of the streamline will be a constant value that is equal to the wedge angle that produces the given bow-shock angle for the given design Mach number.

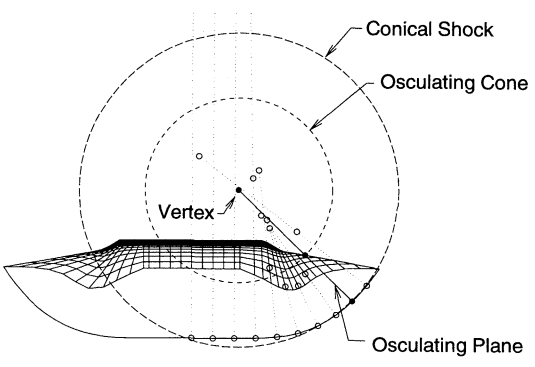

Fig. 1 Method of osculating cones.[28]

Inverse Design and Optimization

One of the most important characteristics of the waverider design is that it is an inverse design, in which a desired flowfield is first selected and then a shape that produces the generated flowfield is determined. The power of the inverse design technique is particularly evident for a fully integrated waverider vehicle design. For instance, in the engine/airframe integration concepts proposed for use with scramjet engines, the waverider forms the vehicle forebody, which acts as part of the engine inlet. For combustion to take place, the engine flow must meet certain requirements. Because the generating flowfield can be prescribed, the waverider forebody can deliver precisely desired thermodynamic and kinematic conditions into the engine. Also, because the aerodynamic forces can be calculated accurately with efficiency, many different parametric studies can be performed on a wide range of integrated vehicles with very little computational effort.

For any given generating flowfield, an infinite number of waveriders can be selected by varying the shock-intersection curve. For the osculating cone waverider design, the shockwave shape can also be varied. Furthermore, on a waverider-based vehicle design, the design of the propulsion system and the aftbody shape can be varied as well. Thus, an optimizer can be used to select the best shape among many, where best is defined by some objective function that can relate either to the pure aerodynamic form or an integrated performance parameter. In this study, the sequential quadratic programming method as implemented by *Design Optimization Tools* available through VMA Engineering, is used to optimize the design for maximum cruise-range performance.[16]

The gradients used in the algorithm are calculated using finite differences by the optimization code. Even for a highly interdisciplinary design, the number of variables required to define a waverider are limited and the objective function is readily calculated by analytical means, and so the cost of calculating the finite differenced gradients is not severe.

Vehicle Model

Figure 2 shows a representative vehicle design generated by the present vehicle model. An osculating cone waverider forms the forebody as well as a portion of the airframe. The forebody is designed to supply the inlet with uniform flow. The leading edge of the waverider is defined by a third-degree Bezier curve. A compression surface, which is defined by polynomial curves, forms the top surface of the forebody. The forebody connects to a two-dimensional, three-stage inlet ramp. The angles and the lengths of the forebody and ramps are such that all shocks are focused on the cowl lip at the cruise flight condition. The throat of the inlet is located at the intersection of the reflected cowl shock and the body keel line. The variable cowl is assumed to translate at off-design conditions to maintain shock cancellation at the throat. The surface of the airframe aft of the waverider section is defined by various polynomial curves. The aft section of the vehicle is faired such that it forms zero base area. The control-surface design is based on the control surface designed for the McDonnell Douglas DF-2 design.[30]

The hydrogen scramjet engine is modeled with a constant area section with a linear divergence section as shown in Fig. 2. The flow through the scramjet is assumed to be quasi-one-dimensional, and the flow properties are calculated using Shapiro's[31] influence coefficients. The details of fuel mixing and ignition are ignored, and the variation of the reacting fuel equivalence ratio is represented by a rational function given by[32]

$$\frac{\phi_r}{\phi} = \frac{\theta_h(x/x_l)}{1 + (\theta_h - 1)(x/x_l)} \tag{1}$$

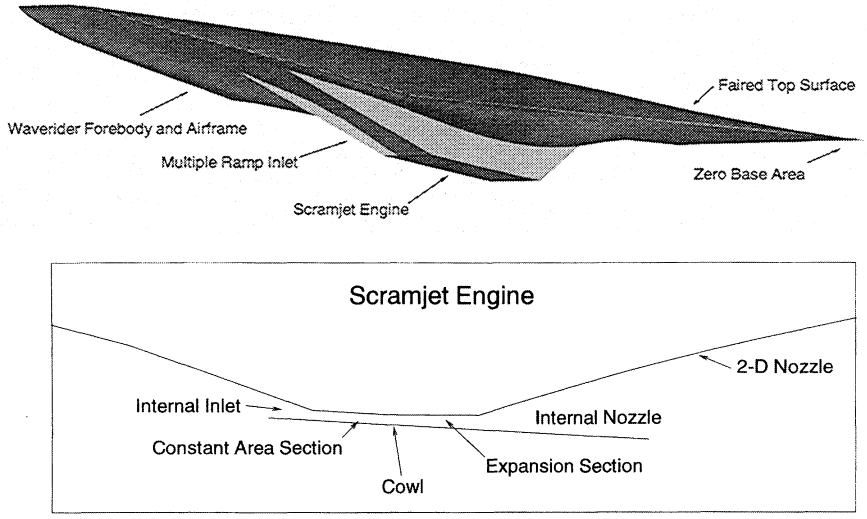

Fig. 2 Perspective view of the waverider-based hypersonic vehicle design and a close-up of the scramjet channel.

where x is the length measured from the fuel-injector location. The values of θ_h, which determines the heat release profile, and characteristic length x_l, depend on the detailed design, placement, and total number of injectors present in the combustor section. It is beyond the scope of the present work to specify the actual design of the fuel-injection system, and so a single representative value is used for θ_h and x_l to model the gross behavior of a perpendicular fuel-injection system. Based on previous work,[9] the mixing length is set to be 2 m. The value of θ_h is chosen to be 9 to match an experimental distribution for perpendicular injection.[33] A conservative mixing efficiency of $\eta_{\text{mix}} = 0.75$ is used to account for incomplete combustion.[34] The mixing efficiency is defined as the ratio of reacted fuel to added fuel. At a given location downstream of the injector, the chemical equilibrium composition of the flow is calculated using the upstream pressure and temperatures. The specific heats c_p and c_v are calculated by finite differencing the enthalpy and internal energies, which are, in turn, used to calculate the specific heat ratio.

The thermodynamic properties at the combustor exit are used as inputs to calculate the nozzle flow. The overall nozzle is formed by internal and external nozzles. The two-dimensional nozzle flow is calculated using the method of characteristics. Once the internal nozzle flow is calculated, an iterative scheme is used to calculate the shape of the slip line between the exhaust and freestream flows, and the plume shock. The flow bounded by the nozzle wall and the slip line is assumed to be frozen, and the specific heat ratio calculated by the combustor model is used throughout this flow.

Force Calculation

Because the waverider surface is defined by streamlines that lie between a shock and a surface, the surface-pressure predictions made by both the tangent-wedge and tangent-cone methods match the exact pressure the distribution poorly, as shown in Fig. 3. Figure 3 shows that the tangent-wedge method underpredicts, and that the tangent-cone method overpredicts, the pressure distribution along the centerline of a Mach 6 waverider.

To accurately predict the surface flow properties, a hybrid method of tangent-wedge and tangent-cone methods is used. The method, which was suggested by Bowcutt and described by Grantz,[35] uses the conical flow solution for the given freestream Mach number. From the conical flow solution, a relationship is obtained between the local streamline deflection angle and the various flow properties such as pressure, density, Mach number, etc. A cubic-spline is performed for two flow variables and the Mach number. The local surface inclination

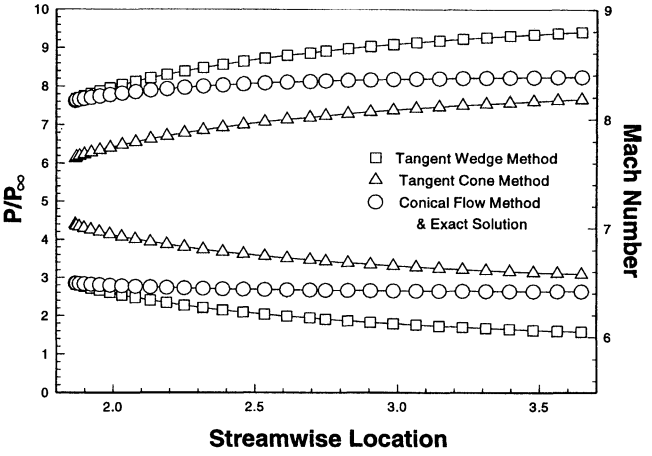

Fig. 3 Comparison of the local surface-inclination methods.

is calculated in the plane of the constant azimuthal angle. The exact inviscid surface flow properties can be then obtained at the on-design condition. Because the flow remains nearly axisymmetric,[26] the same technique can be applied at the off-design hypersonic conditions.

For the rest of the airframe, the surface properties are calculated using the shock-expansion method. The viscous forces on all of the surfaces are calculated using a reference temperature method.[36] The flow is assumed to be entirely turbulent and the wall temperature is held constant at 1000 K on the entire airframe.

To validate the force predictions, Euler calculations have been performed on a Mach 10 vehicle,[29] designed by the present vehicle model. The General Aerodynamic Simulation Program[37] (GASP) is used to solve the Euler equations with a space-marching technique. Calculations are made on the waverider forebody at angles of attack from -6 to $+6$ deg, in 2-deg increments, at the design Mach number of 10 and at off-design freestream Mach numbers of 4, 6, and 8 at zero-deg of angle of attack. Figures 4 and 5 show the variation of forebody L/D with angles of attack and freestream Mach number as predicted by the design code and calculated from the numerical calculation. For the numerical calculation, the viscous force is calculated using the same reference temperature method in the design code. The two results are in excellent agreement. The difference for the Mach number variation is less than 2%, and for the angle-of-attack variation, with the exception of $\alpha = -4$

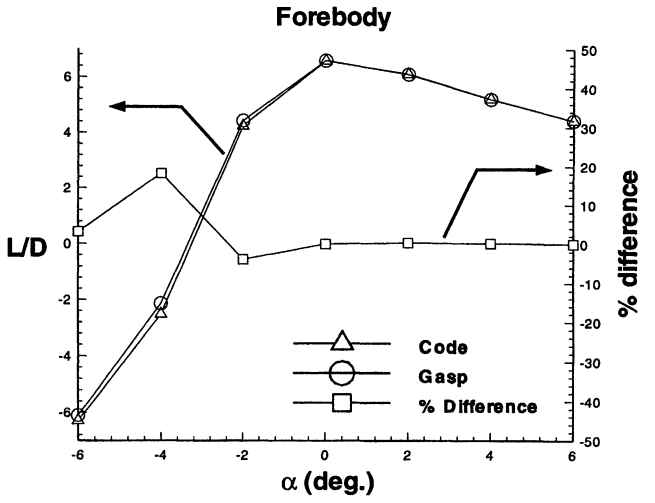

Fig. 4 Forebody L/D variation with α for $M_\infty = 10$.

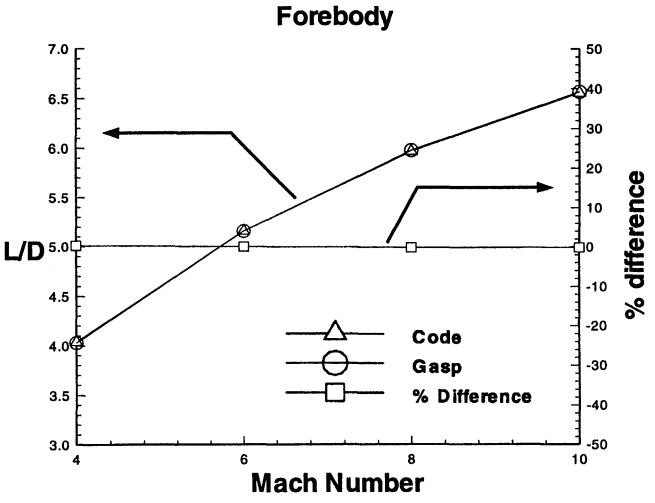

Fig. 5 Forebody L/D variation with M_∞ at $\alpha = 0$.

deg, where the L/D approaches zero at $\alpha = -3.25$ deg, the difference is less than 5%.

Figures 6 and 7 compare the inviscid pressure contours on the surface of the airframe predicted by the design code and calculated by GASP. Because the flow is assumed to be two dimensional in the vehicle model, the effects of flow spillage from the inlet and nozzle on the surface flow are neglected by removing the inlet ramps and the propulsion system in the calculation. The contour lines are both qualitatively and quantitatively in good agreement.The design code predicts the inviscid L/D of the airframe to be 7.81 vs 7.32 for the computational results, which is a 6.3% difference.

Methodology

A total of 18 design variables are used to define the geometry of the vehicle. The design variables are shown in Fig. 8, and Table 1 lists the name and description of the design variables. A value of 124 kg/m^3, reported by Ardema et al.,[38] to represent the mass of a hydrogen-fueled hypersonic waverider vehicle, is used for the average body density.[39] The fuel-volume fraction based on the total volume is chosen from results of the NASA dual-fuel vehicle design study. The percentage of the fuel volume is assumed to be 55% of the total volume, of which 10% is for JP7 and the rest is for liquid hydrogen. The length of the vehicle is set at 60 m.

The design is optimized for maximum range along a constant dynamic pressure trajectory of 1000 psf, starting from Mach 6 and ending at a Mach 10 cruise. Table 2 summarizes the freestream conditions at the various Mach numbers. For M_∞ less than 10, the fuel-equivalence ratio is 1.0, and 0.5 for the cruise condition. To avoid choking the combustor flow at lower hypersonic speeds, the constant for the rational function that specifies the fuel-equivalence ratio profile is linearly increased with M_∞ from 2 to 9. The aerodynamic and the propulsion forces are calculated along the trajectory at five discrete freestream Mach numbers from Mach 6 to Mach 10 in increments of one Mach number.

At each point, the vehicle performance is calculated for $\alpha = 0$ and -1 deg, to determine the $L = W$ angle of attack. The L/W is calculated for each angle of attack, and assuming linear variation, the angle of attack that gives $L/W = 1$ is determined. The performance is then calculated for this angle of attack.

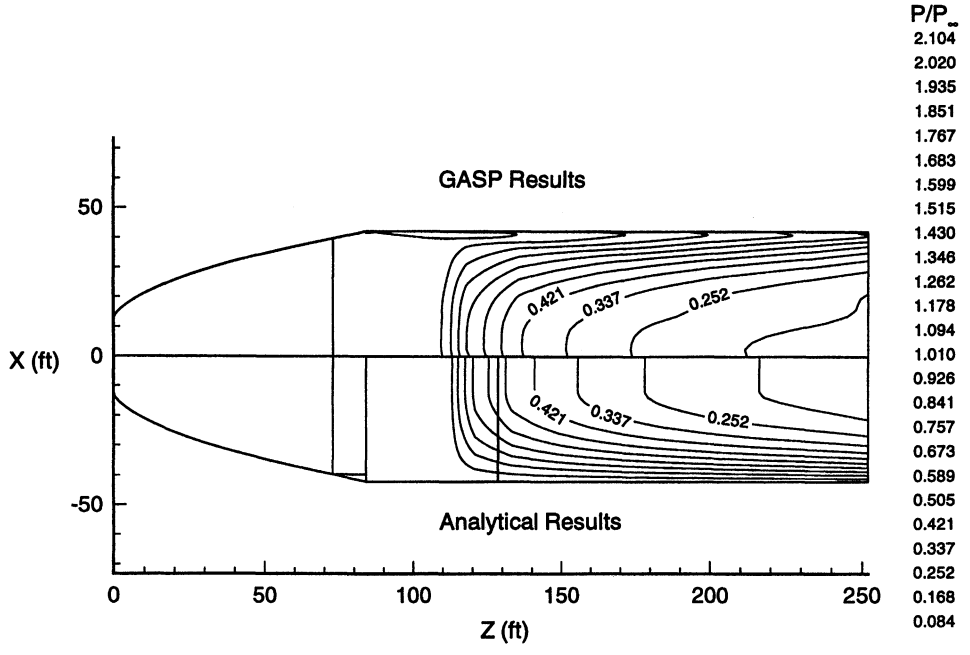

Fig. 6 Comparison of pressure contours on the top surface of the DF-2 airframe calculated by the analytical method and GASP inviscid calculation ($M_\infty = 10$ and $\alpha = 0$).

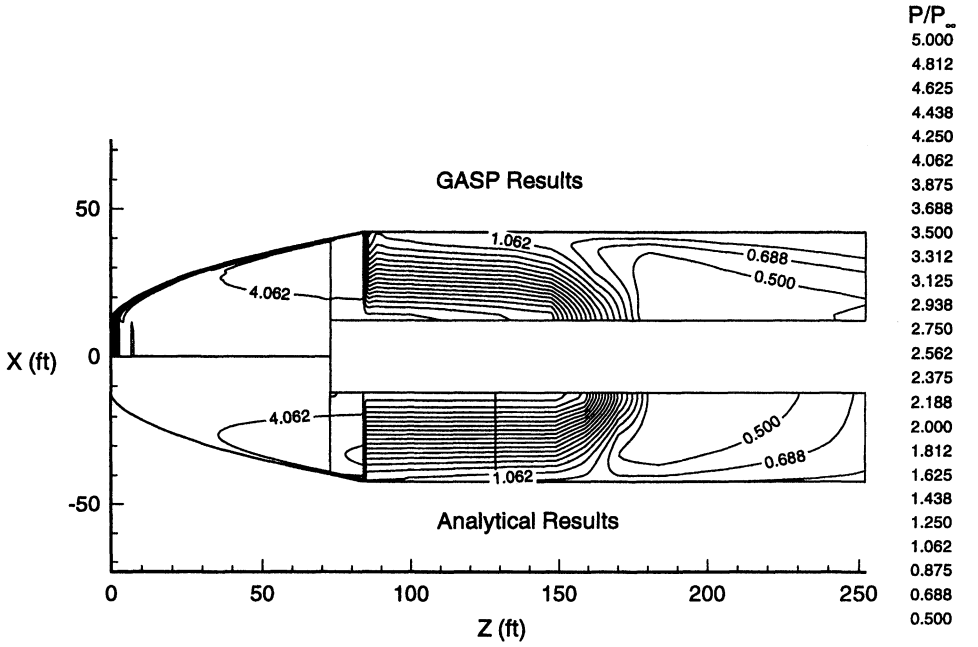

Fig. 7 Comparison of pressure contours on the bottom surface of the DF-2 airframe calculated by the analytical method and GASP inviscid calculation ($M_\infty = 10$ and $\alpha = 0$).

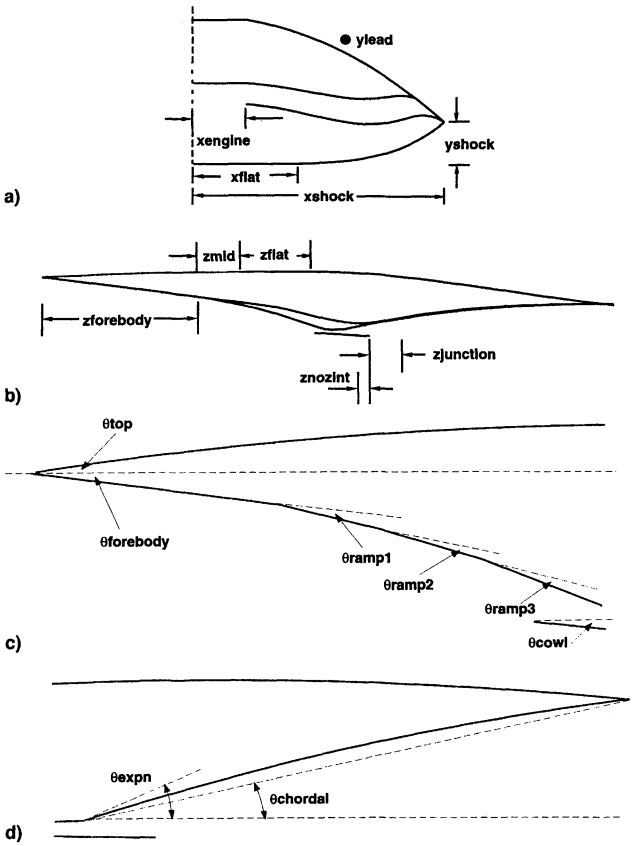

Fig. 8 Design variables: a) waverider cross section, b) vehicle profile, c) close-up of the forebody and inlet ramps, and d) close-up of the aft body and nozzle.

The aerodynamic and the propulsion forces are calculated at discrete Mach numbers. The net thrust is determined, and the instantaneous acceleration is given by

$$a_i = (T_{\text{net}_i} + V_{\infty_i}\dot{m}_{f_i})/m_i \tag{2}$$

where the indice i indicates discrete freestream condition. By assuming constant acceleration and constant freestream temperature, the time it takes to accelerate to the next discrete Mach number is simply

$$\Delta t_i = [(M_{\infty_{i+1}} - M_{\infty_i})\overline{\gamma RT_{\infty_i}}]/a_i \tag{3}$$

Then the distance covered during this time is

$$\Delta R_i = \tfrac{1}{2}a_i\Delta t_i^2 + V_{\infty_i}\Delta t_i \tag{4}$$

The weight of the vehicle is updated by

$$W_{i+1} = W_i - \dot{m}_{\text{fuel}_i}\Delta t_i \tag{5}$$

By summing the discrete distances and range calculated for the cruise condition ion, which is given by

$$R_{\text{cruise}} = 2\frac{\overline{2}}{\rho_\infty S_{\text{ref}}} I_{\text{sp}} \frac{\overline{C_L}}{C_D}(\overline{W_0} - \overline{W_1}) \tag{6}$$

the total range of the vehicle along the hypersonic trajectory can be calculated.

Along the entire trajectory, the total pitching moment of the vehicle is constrained to be zero, and at the cruise condition, thrust equals drag and the initial cruise weight equals the total lift, which includes orbital relief, with zero angle of attack. The takeoff gross weight (TOGW) is limited to 500,000 lb (227,000 kg), following the example of the NASA dual-fuel vehicle design.[2] In addition, the design must satisfy the following geometric constraints:

1) Waverider length constraint: The length of the waverider section is constrained to be less than or equal to half the vehicle length. This is to ensure that there are no invalid waverider designs within the design space:

$$(\text{zforebody} + \text{zmid}) \leq 0.5 \tag{7}$$

2) Nozzle exit height constraint: The height of the nozzle exit is constrained to be less than or equal to 95% of the height of the nose, measured from the osculating shock.[40] This is to

Table 1 Design variables

Variable name	Description
xshock	Semiwidth of the vehicle
yshock	Defines the height of the shock wave
xflat	Defines the width of the planar shock
xengine	Defines the width of the engine
ylead	Leading-edge variable
zforebody	Length of the forebody
zmid	Defines the length of the waverider
zflat	Defines the length of the faired top surface
zjunction	Defines the nozzle/lower surface junction point
$\theta_{chordal}$	Nozzle chordal angle
θ_{expn}	Initial expansion angle of the nozzle
znozint	Defines the length of the internal nozzle
$\theta_{forebody}$	Angle of the forebody
θ_{top}	Angle of the compression angle on the top surface
θ_{ramp1}	Angle of the first ramp
θ_{ramp2}	Angle of the second ramp
θ_{ramp3}	Angle of the third ramp
θ_{cowl}	Cowl inclination angle

Table 2 Freestream conditions for q_∞ = 1000-psf trajectory

M_∞	h, km	P_∞, N/m^2	T_∞, K
6	26.8	1900	222
8	30.7	1069	233
10	33.8	654	242

ensure that the aftbody design remains valid within the design space:

$$\text{ynozzle/ynose} \leq 0.95 \tag{8}$$

3) Combustor location constraint: The location of the cowl leading edge is constrained to be between 50 and 55% of the vehicle length. This is to ensure that the final design has a reasonable location for the center of gravity and combustion system:

$$0.50 \leq \text{zcowl} \leq 0.55 \tag{9}$$

4) Planar shock width constraint: The width of the planar section of the shock is constrained to be greater than 75% of the engine width to ensure engine flow uniformity. Note that 100% is not chosen because it increases the range of valid waverider designs without substantially affecting the engine flow uniformity:

$$\text{xflat/xengine} \geq 0.75 \tag{10}$$

5) Anhedral angle constraint: The minimum difference between the angles of the slope of the leading edge curve and the slope of the osculating plane at the tip is constrained to be 5 deg to avoid invalid designs.

6) Forebody angle constraint: So that the leading edge of the forebody does not become excessively thin, the angle of the forebody at the leading edge is constrained to be greater than a representative value of 6 deg:

$$\theta_{forebody} + \theta_{top} \geq 6 \text{ deg} \tag{11}$$

7) Cowl inclination angle constraint: The inclination angle of the cowl is set to be equal to half of the forebody leading-edge angle. This is done so that the cowl becomes aligned approximately to the freestream when the vehicle is pitched to zero forebody lift:

$$\theta_{cowl} = 0.5(\theta_{forebody} + \theta_{top}) \tag{12}$$

8) Ramp angle constraints: The angles of the ramps are constrained such that successive ramps have a smaller turning angle than the previous ramps. This is done to minimize the chance of flow separation on the inlet ramps:

$$\theta_{ramp2} \leq \theta_{ramp1} \tag{13}$$

$$\theta_{ramp2} \leq \theta_{ramp2} \tag{14}$$

The weight of the vehicle at the beginning of the hypersonic trajectory is calculated based on the following assumptions:

1) Total fuel volume is 55% of the total volume.

2) Hydrogen fuel volume is 90% of the total fuel volume.

3) Hydrocarbon fuel volume is 10% of the total fuel volume.

4) Initial weight = (empty weight) + (H_2 fuel weight) + 0.25[hydrocarbon (HC) fuel weight].

5) Final weight = (empty weight) + 0.25(HC fuel weight).

ρ_{H_2} = 4.74 lb/ft^3 and ρ_{HC} = 49.5 lb/ft^3 are used to calculate the weight of the fuel. The volume fractions are based on the analysis performed by the McDonnell Douglas Corporation on the DF-2 vehicle design.[2,3,29]

For comparison purposes, a design is also optimized for maximum cruise range for a fixed Mach 10 cruise condition listed in Table 2. This design is also subject to the same constraints that are imposed on the design optimized for the entire trajectory, and the same initial weight is also used.

Results

The following is a list of the performance of the maximum hypersonic range designs at Mach 10: airframe C_L = 0.0313, control-surface C_L = −0.00083, propulsion C_L = −0.00157, airframe C_D = 0.00829, control-surface C_D = 0.00002, C_T = 0.00825, airframe C_M = 0.00509, propulsion C_M = −0.00474, control-surface C_M = −0.00035, airframe L/D = 3.78, I_{sp} = 2705 s, total range = 7296 nm, and cruise range = 8345 nm. Various views of the optimized design are shown in Figs. 9 and 10. The optimized design satisfies all of the constraints;

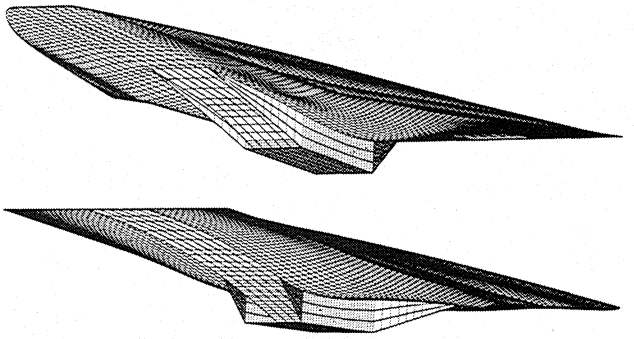

Fig. 9 Front and rear quarter views of the maximum hypersonic-range design.

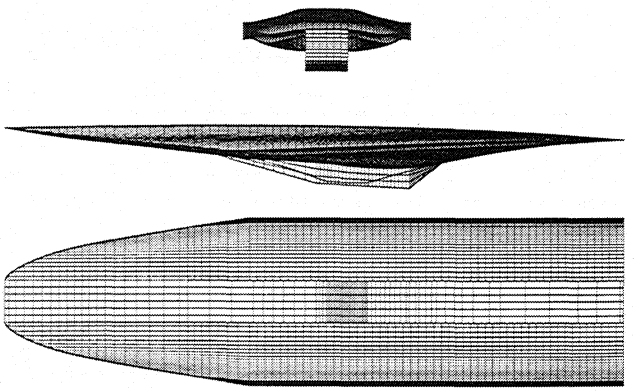

Fig. 10 Three views of the maximum hypersonic-range design.

however, the following constraints are active: 1) maximum nozzle height, 2) minimum cowl leading-edge location, 3) ramp-angle constraints, and 4) maximum TOGW. Because the ramp turning angles are constrained to successively decrease toward the engine, the active constraints on the ramp angles indicate that the angle of the third ramp is the maximum feasible value. The advantage of a greater turning angle for the third ramp is that it will reduce the nose-up pitching moment by shifting the greater portion of the inlet pressure rise closer to the vehicle's center of gravity. The greater turning angle for the third ramp also moves the cowl's leading-edge forward as a result of the shock-on-lip design condition. This also moves the combustor section forward, thereby increasing the nozzle length and its height. The maximum TOGW contributes to a better cruise-range performance because of greater available fuel weight.

The design of the vehicle is very similar to the design optimized for maximum cruise range at a single design point of $M_\infty = 10$. Table 3 lists and compares key geometry elements of the maximum cruise-range design with the maximum hypersonic-range design.

To compare the performance of the two designs, the hypersonic range for the cruise-range-optimized design along the same trajectory is calculated. Figure 11 shows the distance covered along the hypersonic trajectory for the two designs. This plot shows that the distance covered while accelerating from Mach 6 to the Mach 10 cruise is less than 15% of the total distance covered along the hypersonic trajectory.

Table 3 Comparison of geometry designs of maximum cruise-range design with the maximum hypersonic-range design

Design parameter	Cruise-range design	Total-range design	% diff.
Forebody length	18.0 m	17.7 m	1.69
Waverider length	23.3 m	23.7 m	−1.68
Compression surface length	32.5 m	23.7 m	40.1
Center of volume	33.2 m	33.2 m	0.00
Vehicle width	16.0 m	16.5 m	−3.03
Nose/engine width	4.27 m	4.17 m	2.40
θ_δ	2.2 deg	1.7 deg	29.4
θ_{comp}	0.480 deg	0.696 deg	−31.0
Forebody angle	6.10 deg	5.73 deg	6.46
First ramp angle	4.61 deg	4.70 deg	−1.91
Second ramp angle	4.61 deg	4.70 deg	−1.91
Third ramp angle	4.61 deg	4.70 deg	−1.91
Cowl angle	3.29 deg	3.21 deg	2.49
θ_{expn}	18.000 deg	18.000 deg	0.00
θ_{nozzle}	13.0 deg	13.0 deg	0.00
Internal nozzle length	4.0 m	4.0 m	0.00
Wetted area	1823 m^2	1861 m^2	−2.04
Planform area	864.0 m^2	886.7 m^2	−2.56
Maximum cross-sectional area	57.4 m^2	57.2 m^2	0.35
TOGW	226,568 kg	226,651 kg	0.04

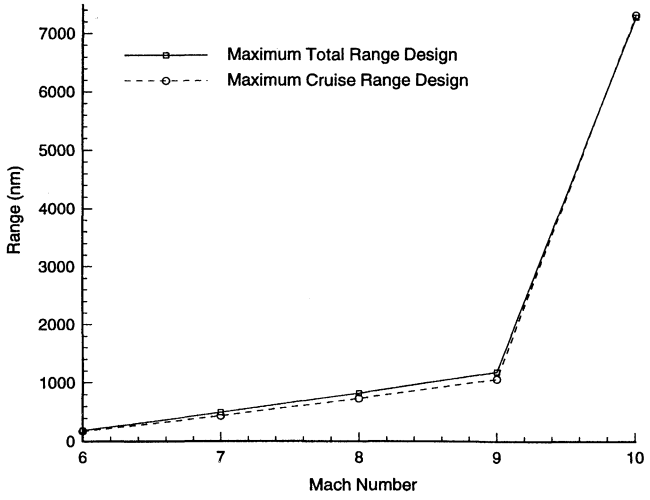

Fig. 11 Range performance of the maximum hypersonic-range design and the maximum cruise-range design.

Figure 12 shows the angle of attack and control-surface deflection angle for the two designs along the trajectory. The variations of angle of attack and control-surface deflection are nearly identical between the two designs. The magnitude of the angle of attack of the maximum cruise-range designs are greater than the maximum hypersonic-range design. The angle of attack of the maximum cruise-range design is negative at the cruise Mach number because the specified design flight weight of the vehicle is greater than the calculated weight at Mach 10. This means that the maximum cruise-range design has L/W greater than unity at a Mach 10 cruise condition; hence, a negative angle of attack is necessary to cancel the excess lift. In contrast to the angle of attack, the magnitude of the control-surface deflection is greater for the maximum hypersonic range design. For both designs, the control-surface deflection is greatest at Mach 6. The deflection angles decrease as the Mach increases until negative deflection angles are predicted for both designs at Mach 9. At the cruise condition, both designs once again have positive control-surface deflection angles.

Table 4 lists the distance covered during each segment and the hypersonic range for the two designs. The design optimized for hypersonic range covers an 11.5% greater distance during the acceleration phase than the design optimized for cruise range. The percent difference between the distances covered is greatest at 12.4% for the Mach 6 to Mach 7 segment; however, because the maximum hypersonic range is not specifically optimized for the cruise condition, the design optimized for cruise range covers a 2.58% greater distance at the cruise condition than the maximum hypersonic range design. In the end, the total range of the maximum hypersonic range design is 7296 nm, which is <1% smaller than the hypersonic range of the maximum cruise-range design.

The starting weight at the cruise condition, weight of fuel available, I_{sp}, thrust, and fuel equivalence ratio for the two designs are listed in Table 5. This table shows that the greater I_{sp}, lift, and weight of fuel available accounts for the better cruise-range performance of the maximum cruise-range design. For the maximum cruise-range design, when the angle of attack is set negative to match the lift to the weight of the vehicle, the decrease in the vehicle drag is greater than the decrease in thrust. Thus, the vehicle has excess thrust at the cruise condition. To match the thrust to drag, the fuel flow is decreased to match the thrust to the decreased drag. This ac-

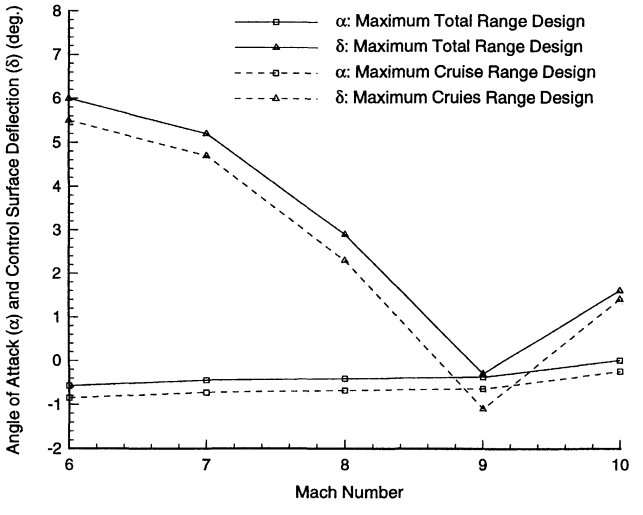

Fig. 12 Angle of attack and control-surface deflection variation of the maximum hypersonic-range design and the maximum cruise-range design along the hypersonic trajectory.

Table 4 Comparison of range performance through trajectory

Flight segment	Cruise-range design	Total-range design	% difference
Mach 6 to Mach 7	176	201	−12.4
Mach 7 to Mach 8	263	296	−11.1
Mach 8 to Mach 9	295	328	−10.1
Mach 9 to Mach 10	327	359	−8.91
Mach 10 cruise	6271	6113	2.58
Total range	7332	7296	0.49

Table 5 Comparison of two designs

Parameter	Cruise-range design	Total-range design	% difference
W_0, lb	343,211	341,196	0.59
W_{fuel}, lb	99,801	97,696	2.15
I_{sp}, s	2752	2705	1.74
Thrust, N	358,822	352,822	1.70
ϕ	0.475	0.50	−5.00

counts for the increased I_{sp} from the design value of 2700–2760 s. Also, the greater thrust margin of the maximum cruise-range design contributes to slightly greater available fuel at the cruise condition. These two factors are the reason for the maximum cruise-range design having a greater hypersonic range than the maximum hypersonic-range design. However, the results of this comparison are misleading because the maximum cruise-range design violates the design parameter constraints applied to the maximum hypersonic-range design. In addition to the different fuel equivalence ratios, the height of the maximum cruise-range design is the maximum allowable value, so that by flying at a negative angle of attack, that constraint is violated. Furthermore, the cowl inclination angle for the maximum hypersonic-range design is constrained to be half of nose angle, which is no longer the case when the vehicle is pitched.

Conclusions

A hypersonic vehicle model based on waverider shapes derived from the method of osculating cones has been developed. The osculating cone's waverider forebody has been specifically designed to produce uniform flow for the two-dimensional engine design. The vehicle model has been validated with numerical calculations. The vehicle model has been used to optimize an overall design for a fixed Mach 10 cruise-range performance and maximum range along a constant dynamic pressure trajectory of 1000 psf (47.8 kPa), starting from Mach 6 to Mach 10 cruise flight. The angle of attack is varied and the control surfaces are deflected to maintain $L = W$ and zero-pitching moment along the trajectory. The variation of angles of attack is <1 deg and the maximum control-surface deflection angle that occurs at Mach 6 is <7 deg.

The hypersonic range calculated for the maximum cruise-range design is found to be virtually identical to the range performance of the design optimized for the entire trajectory; however, the design optimized for the trajectory covers a greater range from Mach 6 to Mach 10 than the maximum cruise range. The maximum cruise-range design covers a greater range at cruise condition, with more available fuel at the start of the cruise flight and better I_{sp} to make up the deficit, but for the maximum cruise-range design to fly at steady state, the vehicle requires a −0.25-deg angle of attack and a fuel equivalence ratio of 0.475. The change in the angle of attack and fuel equivalence ratio from the original design of $\alpha = 0$ deg and $\phi = 0.5$ is a result of the difference in the weight of the vehicle at the beginning of the cruise condition from the original design specification. The reduction in the initial weight at the cruise requires the vehicle to fly at a small negative angle of attack. This results in a reduction in drag that is balanced by lower thrust with reduction in the fuel flow, and hence, better cruise range.

The width of the engine on the maximum hypersonic range design is 2.4% less than the maximum cruise-range design. This is in contrast to the designs that were optimized for acceleration in previous studies.[39,40] Generally, vehicle designs that are optimized for acceleration have a greater engine width than corresponding designs optimized for cruise, and because the design optimized for the hypersonic trajectory has to accelerate from Mach 6 to Mach 10, a similar trend had been expected. However, because the design is optimized for the hypersonic range rather than for the cruise range, and it must also satisfy steady-state flight constraints with the specified design parameters, the end result is a vehicle design that covers a greater range while accelerating at a slower rate to the cruise Mach number, and which matches the vehicle weight and the lift it produces at the beginning of the cruise condition.

The differences in the geometry and the hypersonic range performance between waverider-based Mach 10 cruise vehicle designs optimized for maximum cruise range and hypersonic range along a hypersonic trajectory are found to be small. This result is encouraging because more than 10 times the CPU time is required to obtain a converged solution for the design optimized along the hypersonic trajectory than that for a fixed cruise condition, which leads to a significant reduction in the computational time needed to find an optimized design. The savings in the computational time can be allocated for performance analysis at lower speeds; however, the angle of attack and the fuel equivalence ratio had to be modified from the original design specification for the maximum cruise-range design to fly steady state at the cruise flight condition. The angle of attack was decreased to match the lift-to-weight, and the fuel flow rate was also decreased to match the thrust-to-drag. The minimum allowable fuel equivalence ratio for a hypersonic cruise vehicle may be dictated by the cooling requirements on the vehicle and not by the engine performance; hence, reducing the fuel flow rate from the designated value may not be possible for this design. So, while the performance and the geometry of the two designs are similar, the single point optimized design may not be feasible because of other constraints not considered for the present study.

Acknowledgments

This work was supported in part under NASA Grant NAGW-3175, with Isaiah M. Blankson as the Program Monitor. I. M. Blankson has also contributed many thoughts and suggestions in this work, for which appreciation is expressed. Appreciation is also expressed to Mary Kae Lockwood of NASA Langley Research Center, Darryll Pines of the Department of Aerospace Engineering at the University of Maryland, and Christopher Tarpley of the Astrox Corporation for their contributions as well. Thanks are also extended to Tom Bogar, Don Johnson, and Ed Eiswirth of the Boeing Corporation Phantom Works for contributing important suggestions and insights into hypersonic vehicle design.

References

[1]Swithenbank, J., "Hypersonic Air-Breathing Propulsion," *Progress in Aeronautical Sciences*, Vol. 8, 1967, pp. 229–294.

[2]Hunt, J., and Eiswirth, E. A., "NASA's Dual-Fuel Airbreathing Hypersonic Vehicle Study," AIAA Paper 96-4591, Nov. 1996.

[3]Bogar, T., Alberico, J., Stemler, J., and Espinosa, A., "Dual Fuel Lifting Body Configuration Development," AIAA Paper 96-4592, Nov. 1996.

[4]Spall, R., and Malik, M. R., "Effect of Transverse Curvature on the Stability of Compressible Boundary Layers," *AIAA Journal*, Vol. 29, No. 9, 1991, pp. 1596–1602.

[5]Weber, R. J., and MacKay, J. S., "An Analysis of Ramjet Engines Using Supersonic Combustion," NASA TN4386, Sept. 1958.

[6]Ferri, A., "Review of Problems in Application of Supersonic Combustion," *Journal of the Royal Aeronautical Society*, Vol. 68, Sept. 1964, pp. 575–595.

[7]Rogers, R. C., and Schexnayder, C. J., Jr., "Chemical Kinetic Analysis of Hydrogen-Air Ignition and Reaction Times," NASA TP 1856, July 1981.

[8]Paull, A., Stalker, R., and Mee, D., "Experiments on Supersonic Combustion Ramjet Propulsion in a Shock Tunnel," *Journal of Fluid Mechanics*, Vol. 296, Aug. 1995, pp. 159–183.

[9]O'Neill, M. K., and Lewis, M. J., "Design Tradeoffs on Scramjet Engine Integrated Hypersonic Waverider Vehicle," *Journal of Aircraft*, Vol. 30, No. 6, 1993, pp. 943–952.

[10]O'Neill, M. K., and Lewis, M. J., "Airbreathing Hypersonic Vehicle Design and Analysis Methods," AIAA Paper 91-0381, Jan. 1991.

[11]Raney, D., McMinn, J. D., and Pototzky, A., "Impact of Aeroelastic-Propulsive Interactions on Flight Dynamics of a Hypersonic Vehicle," *Journal of Aircraft*, Vol. 32, No. 2, 1995, pp. 355–362.

[12]McQuade, P. D., Eberhardt, S., and Livne, E., "CFD-Based Aerodynamic Approximation Concepts Optimization of a Two-Dimensional Scramjet Vehicle," *Journal of Aircraft*, Vol. 32, No. 2, 1995, pp. 262–269.

[13]Payne, J. L., and Walker, M. A., "An Efficient Coupling of a PNS Code and a Parallel Full Navier-Stokes Code for Complex Hypersonic Vehicle Design," AIAA Paper 96-3402, July 1996.

[14]Sabean, J., and Lewis, M. J., "Performance Optimization of a SCRAM Projectile Flying in an External Propulsion Accelerator," *Journal of Propulsion and Power*, Vol. 13, No. 5, 1997, pp. 592–600.

[15]Baysal, O., and Eleshaky, M., "Aerodynamic Design Optimization Using Sensitivity Analysis and Computational Fluid Dynamics," *AIAA Journal*, Vol. 30, No. 3, 1992, pp. 718–725.

[16]Vanderplaats, G. N., "An Efficient Feasible Direction Algorithm for Design Synthesis," *AIAA Journal*, Vol. 22, No. 11, 1984, pp. 1633–1640.

[17]Foster, N., and Dulikravich, G., "Three-Dimensional Aerodynamic Shape Optimization Using Genetic and Gradient Search Algorithms," *Journal of Spacecraft and Rockets*, Vol. 34, No. 1, 1997, pp. 36–42.

[18]Dulikravich, G., and Sheffer, S. G., "Aerodynamic Shape Optimization of Hypersonic Configurations Including Viscous Effects," AIAA Paper 92-2635, June 1992.

[19]Sabean, J., Lewis, M. J., Mee, D., and Paull, A., "Performance Study of a Power Law Star Body," AIAA Paper 98-1617, April 1998.

[20]Kothari, A., Tarpley, C., McLaughlin, T. A., and Babu, E., and Livingston, J. W., "Hypersonic Vehicle Design Using Inward Turning Flow Fields," AIAA Paper 96-2552, July 1996.

[21]Tarpley, C., and Lewis, M., "Stability and Control of Hypersonic Waverider Vehicles," *Journal of Aircraft*, Vol. 32, No. 4, 1995, pp. 795–803.

[22]Nonweiler, T. R. F., "Aerodynamic Problems of Manned Space Vehicles," *Journal of the Royal Aeronautical Society*, Vol. 63, No. 585, 1959, pp. 521–528.

[23]Rasmussen, M. L., and Clement, L. W., "Cone-Derived Waveriders with Longitudinal Curvature," AIAA Paper 84-2100, Aug. 1984.

[24]Emanuel, G., and Park, H.-K., "Idealized Tip-to-Tail Waverider Model," *Proceedings of the 1st International Hypersonic Waverider Symposium*, Univ. of Maryland, College Park, MD, 1990.

[25]Gillum, M., and Lewis, M., "Analysis of Experimental Results on a Mach 14 Waverider with Blunt Leading Edges," *Journal of Aircraft*, Vol. 34, No. 3, 1997, pp. 296–303.

[26]Takashima, N., and Lewis, M. J., "Navier-Stokes Computations of Hypersonic Viscous Optimized Waveriders," *Journal of Spacecraft and Rockets*, Vol. 31, No. 3, 1994, 383–391.

[27]Takashima, N., and Lewis, M. J., "Waverider Configurations Based on Non-Axisymmetric Flow Fields for Engine-Airframe Integration," AIAA Paper 94-0380, Jan. 1994.

[28]Sobieczky, H., Dougherty, F. C., and Jones, K. D., "Hypersonic Waverider Design from Given Shock Waves," *Proceedings of the 1st International Hypersonic Waverider Symposium*, Univ. of Maryland, College Park, MD, 1990.

[29]Takashima, N., and Lewis, M. J., "Waverider Configuration Development for the Dual Fuel Vehicle," AIAA Paper 96-4593, Nov. 1996.

[30]Tarpley, C., Pines, D. J., and Kothari, A. J., "Low-Speed Stability Analysis of the Dual Fuel Waverider Configuration," AIAA Paper 96-4596, Nov. 1996.

[31]Shapiro, A., *The Dynamics and Thermodynamics of Compressible Fluid Flow*, Wiley, New York, 1953.

[32]Heiser, W. H., and Pratt, D. T., *Hypersonic Airbreathing Propulsion*, AIAA Education Series, AIAA, Washington, DC, Sept. 1994.

[33]Rogers, R. C., "Mixing of Hydrogen Injected from Multiple Injectors Normal to a Supersonic Airstream," NASA TN D-6476, Sept. 1971.

[34]Tarpley, C., "The Optimization of Engine-Integrated Hypersonic Waveriders with Steady State Flight and Static Margin Constraints," Ph.D. Dissertation, Univ. of Maryland, College Park, MD, May 1995.

[35]Grantz, A. C., "Calibration of Aerodynamic Engineering Methods for Waverider Design," AIAA Paper 94-0382, Jan. 1994.

[36]Eckert, E. R. G., "Engineering Relations for Heat Transfer and Friction in High-Velocity Laminar and Turbulent Boundary-Layer Flow over Surfaces with Constant Pressure and Temperature," *Transactions of the American Society of Mechanical Engineers*, Vol. 78, No. 8, 1956, pp. 1273–1283.

[37]McGrory, W. D., Slack, D. C., Applebaum, M. P., and Walters, R. W., *GASP Version 2.2*, Aerosoft Inc., Blacksburg, VA, 1993.

[38]Ardema, M. D., Chambers, M. C., Terjesen, E. J., and Roberts, C. D., "Body Weight of Advanced Concept Hypersonic Aircraft," AIAA Paper 91-3180, Sept. 1991.

[39]O'Neill, M. K., and Lewis, M. J., "Optimized Scramjet Integration on a Waverider," *Journal of Aircraft*, Vol. 29, No. 6, 1992, pp. 1114–1121.

[40]Takashima, N., and Lewis, M. J., "Optimized Mission-Oriented Waverider Vehicles with Base Closure," AIAA Paper 96-0810, Jan. 1996.